HHS Public Access

Author manuscript

J Nat Prod. Author manuscript; available in PMC 2024 July 05.

Published in final edited form as:

J Nat Prod. 2023 March 24; 86(3): 582–588. doi:10.1021/acs.jnatprod.2c01030.

Thorectidiol A Isolated from the Marine Sponge *Dactylospongia elegans* Disrupts Interactions of the SARS-CoV-2 Spike Receptor Binding Domain with the Host ACE2 Receptor

David E. Williams,
Department of Chemistry, University of British Columbia, Vancouver, B.C., Canada V6T 1Z1; Department of Earth, Ocean & Atmospheric Sciences, University of British Columbia, Vancouver, B.C., Canada V6T 1Z4

Joel Cassel,
The Wistar Institute, Philadelphia, Pennsylvania 19104, United States

Jin-Lin Zhu,
Department of Chemistry, University of British Columbia, Vancouver, B.C., Canada V6T 1Z1

Jian-Xiong Yang,
Department of Chemistry, University of British Columbia, Vancouver, B.C., Canada V6T 1Z1

Nicole J. de Voogd,
Naturalis Biodiversity Center, 2300 RA, Leiden, The Netherlands

Teatulohi Matainaho,
University of Papua New Guinea, University National Capital District 134, Papua New Guinea

Joseph M. Salvino,
The Wistar Institute, Philadelphia, Pennsylvania 19104, United States

Yan Alexander Wang,
Department of Chemistry, University of British Columbia, Vancouver, B.C., Canada V6T 1Z1

Luis J. Montaner,
The Wistar Institute, Philadelphia, Pennsylvania 19104, United States

Ian Tietjen,
The Wistar Institute, Philadelphia, Pennsylvania 19104, United States

Raymond J. Andersen

Corresponding Authors: **Ian Tietjen** – *The Wistar Institute, Philadelphia, Pennsylvania 19104, United States*; itietjen@wistar.org; **Raymond J. Andersen** – *Department of Chemistry, University of British Columbia, Vancouver, B.C., Canada V6T 1Z1; Department of Earth, Ocean & Atmospheric Sciences, University of British Columbia, Vancouver, B.C., Canada V6T 1Z4*; raymond.andersen@ubc.ca; Fax: 604 822 6091.

Supporting Information

The Supporting Information is available free of charge at https://pubs.acs.org/doi/10.1021/acs.jnatprod.2c01030.
^{1}H, ^{13}C, and 2D NMR spectra of compounds **1, 4, 5**, and **6**; measured and calculated ECD spectra for **4, 5**, and **6** (PDF)

Complete contact information is available at: https://pubs.acs.org/10.1021/acs.jnatprod.2c01030

The authors declare no competing financial interest.

DEDICATION

Dedicated to Dr. Mary J. Garson, The University of Queensland, for her pioneering work on bioactive natural products.

Department of Chemistry, University of British Columbia, Vancouver, B.C., Canada V6T 1Z1; Department of Earth, Ocean & Atmospheric Sciences, University of British Columbia, Vancouver, B.C., Canada V6T 1Z4

Abstract

Thorectidiols isolated from the marine sponge *Dactylospongia elegans* (family Thorectidae, order Dictyoceratida) collected in Papua New Guinea are a family of symmetrical and unsymmetrical dimeric biphenyl meroterpenoid stereoisomers presumed to be products of oxidative phenol coupling of a co-occurring racemic monomer, thorectidol (**3**). One member of the family, thorectidiol A (**1**), has been isolated in its natural form, and its structure has been elucidated by analysis of NMR, MS, and ECD data. Acetylation of the sponge extract facilitated isolation of additional thorectidiol diacetate stereoisomers and the isolation of the racemic monomer thorectidol acetate (**6**). Racemic thorectidiol A (**1**) showed selective inhibition of the SARS-CoV-2 spike receptor binding domain (RBD) interaction with the host ACE2 receptor with an IC_{50} = 1.0 ± 0.7 μM.

Graphical Abstract

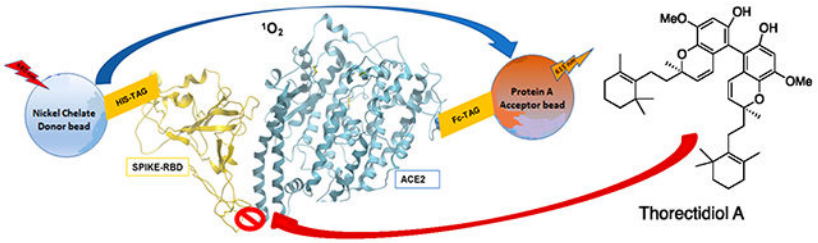

Severe acute respiratory syndrome coronavirus 2 (SARS-CoV-2), the causative agent of Coronavirus Disease 2019 (COVID-19), continues to cause substantial morbidity and mortality worldwide.[1,2] Development of small-molecule therapeutics for the treatment of emerging SARS-CoV-2 variants of concern remains an urgent medical need.[3,4] SARS-CoV-2 gains entry to host cells in part through binding of the viral spike protein receptor binding domain (RBD) to the host angiotensin-converting enzyme II (ACE2) receptor.[5,6] Small molecules that can selectively antagonize this RBD–ACE2 interaction should be useful structural leads for the development of antivirals able to block SARS-CoV-2 infection.

We previously described development of a high-throughput AlphaScreen-based assay that can identify inhibitors of the RBD–ACE2 interaction.[7] The assay uses a SARS-CoV-2 RBD protein containing a C-terminal His tag bound to a nickel chelate acceptor bead and a full-length ACE2 peptide with a C-terminal Fc tag bound to a donor protein A bead. These beads are brought into close proximity as a result of RBD–ACE2 binding, which is monitored by their luminescence at 615 nm when stimulated at 680 nm. Compounds that disrupt the RBD–ACE2 interaction also disrupt the luminescence. An analogous assay comprising the unrelated PD-1-His and PD-L1-Fc host ligand–receptor pair is used as a

counter screen to prioritize small molecules that selectively disrupt the RBD–ACE2 over the PD-1–PD-L1 interaction.

The assay has been used to screen a library of MeOH extracts of marine invertebrates collected in tropical and temperate ocean waters. A MeOH extract of the marine sponge *Dactylospongia elegans* (order Dictyoceratida, family Thorectidae) collected in Papua New Guinea showed promising activity in the screen. Bioassay-guided fractionation of the extract yielded racemic thorectidiol A (**1**), which showed selective inhibition of the RBD–ACE2 interaction over the PD-1–PD-L1 interaction. The thorectidiols are dimeric biphenyl stereoisomers that appear to have been formed via oxidative phenol coupling of the co-occurring racemic meroterpenoid thorectidol (**3**). Details of the isolation, structure elucidation, and biological activities of throectidiol A (**1**) and the acetylated thorectidiol and thorectidol derivatives **4, 5**, and **6** are presented below.

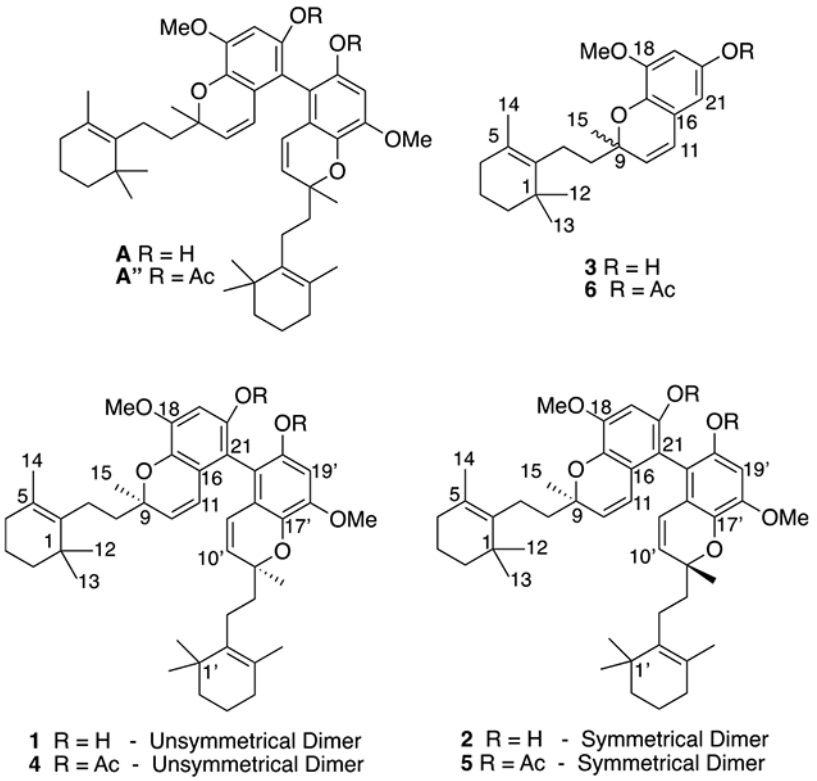

RESULTS AND DISCUSSION

The sponge *D. elegans* was collected by hand using scuba on reefs near Keviang, Papua New Guinea, and frozen on site for transport to Vancouver and long-term storage. Initially, a small portion of the sponge tissue was extracted exhaustively with MeOH to give an extract that was active in the spike protein–ACE2 inhibition assay The dried residue from the MeOH extract was partitioned between H_2O and EtOAc to give a spike/ACE2 inhibitory EtOAc-soluble residue that was fractionated via Sephadex LH-20 chromatography followed by Si gel flash chromatography and then normal-phase HPLC to give a bioactive fraction containing the unsymmetrical dimer thorectidiol A (**1**). Due to the small amount of extract

that was processed in this initial fractionation, no other compounds were obtained in quantities needed for characterization. NMR and MS data collected on this small sample of **1** enabled a tentative assignment of the constitution **A** of this active constituent as outlined below.

Compound **1** was obtained as an optically inactive solid that gave a $[M - H]^-$ ion in the HRESIMS spectrum at *m/z* 681.4157 appropriate for a molecular formula of $C_{44}H_{58}O_6$, requiring 16 sites of unsaturation. Although the compound gave a single clean molecular ion in the HRESIMS and a single peak on normal-phase HPLC, the majority of the ^1H and all the ^{13}C NMR signals in spectra recorded in both C_6D_6 and DMSO-d_6 were doubled in a 1:1 ratio (Tables 1 and 2, Supporting Information). $^1H/^{13}C$/gCOSY/gHSQC/gHMBC NMR data obtained for the sample identified 44 carbon resonances, in agreement with the HRESIMS data. Resonances could be assigned to eight aliphatic methyl singlets, 10 aliphatic methylenes, two phenolic OHs, two aromatic methoxy residues, two oxygen-bearing tertiary aliphatic carbons, two quaternary aliphatic carbons, two *cis* disubstituted olefins, and two tetrasubstituted olefins. There were also two aromatic proton singlets that were each assigned to one of two constitutionally identical pentasubstituted benzene rings. As illustrated in Figure 1, it was possible via detailed analysis of the 1D and 2D NMR data acquired in both C_6D_6 and DMSO-d_6 to identify the constitutions of two structurally identical $C_{22}H_{29}O_3$ monomeric fragments that accounted for all of the atoms in the molecular formula. The two benzene rings, the two trimethyl cyclohexene rings, and the two *cis* disubstituted olefins accounted for 14 of the 16 sites of unsaturation required by the molecular formula. A lack of ^{13}C NMR evidence for additional unsaturated functional groups required that the remaining two sites of unsaturation had to be rings.

A biphenyl bridge between C-21 and C-21′ was supported by the carbon chemical shifts at δ 111.7 and 106.3 assigned to C-21 and C-21′,[8] with the two remaining sites of unsaturation satisfied by ether bridges between C-9 and C-17 and C-9′ and C-17′ to give the thorectidiol constitution **A**. The alternative constitution with ether bridges between C-9 and C-17′ and C-9′ and C-17 generates a structure containing two strained nine-membered rings rather than the two unstrained tetrasubstituted 3,6-dihydro-2*H*-pyran rings assigned to thorectidiol A (**1**).

Biphenyls that have unsymmetrical substitution patterns on each of the phenyl rings and hindered rotation around the single bond that joins the phenyl rings exist as stable atropisomers.[9] The thorectidiol skeleton **A** has the required unsymmetrical substitution patterns on the two biphenyl rings, and, furthermore, the functionality around the C-21/C-21′ thorectidiol bond strongly resembles the functionality around the single bond linking the naphthalene fragments in BINOL, where there is restricted rotation around the bond and atropisomerism. Therefore, there should be no free rotation about the C-21/C-21′ bond in the thorectidiols, leading to the existence of stable atropisomers. In addition to atropisomerism, the thorectidiol skeleton **A** also has two tetrahedral carbon-based stereogenic centers, and, therefore, the possibility of a maximum of eight stereoisomers [9*R*,9′*R*,R_a; 9*R*,9′*R*,S_a; 9*R*,9′*S*,S_a; 9*S*,9′*R*,S_a; 9*S*,9′*S*,S_a; 9*S*,9′*S*,R_a; 9*R*,9′*S*,R_a; and 9*S*,9′*R*,R_a] exists as shown in Figure 2. Closer examination of these eight possible stereoisomers shows that the members of each 9*R*,9′*S*,S_a and 9*S*,9′*R*,S_a pair (**1a**) and

9*R*,9′*S*,R_a and 9*S*,9′*R*,R_a pair (**1b**) can be superimposed on each other via a 180° rotation about an axis perpendicular to the center of the C-21/C-21′ bond followed by a 90° rotation about the C-21/C-21′ bond axis (Figure SI1). Therefore, there are only six possible thorectidiol stereoisomers.

Molecular models show that the thorectidiol stereoisomers with the 9*R**,9′*S** relative configuration [i.e., thorectidiol A (**1**)] have different chemical environments for the C-9 and C-9′ methyl and ethylcyclohexene side chain fragments in the two monomeric units, leading to two sets of ^{1}H NMR resonances in the unsymmetrical dimers. Conversely, the models show that the thorectidiol stereoisomers with the 9*R**,9′*R** relative configurations [i.e., thorectidiol B (**2**) Figure 2] have identical chemical environments for the C-9 and C-9′ methyl and ethylcyclohexene side chain fragments in the two monomeric units, leading to only one set of ^{1}H NMR resonances for the two monomeric fragments in the symmetrical dimers. Therefore, the bioactive thorectidiol A (**1**) sample described above must have the 9*R**,9′*S** relative configuration shown in Figure 2.

A modified workup that involved acetylation of the thorectidiol and thorectidol-containing fractions generated by Si gel chromatography was employed with the remaining portion of the extract to facilitate the isolation and characterization of the additional meroterpenoid natural products. Normal-phase HPLC separation of the acetylated fractions yielded subfractions containing unsymmetrical thorectidiol diacetate **4**, symmetrical thorectidiol diacetate **5**, and thorectidol acetate (**6**). A portion of the pure unsymmetrical dimer thorectidiol A (**1**), obtained initially as described above, was also acetylated, and the purified product was found to be identical by NMR and MS comparison to the unsymmetrical thorectidiol diacetate **4** obtained by purification of the acetylated mixture.

The positive ion HRESIMS data measured for the symmetrical thorectidiol diacetate **5** indicated that the molecular formula was identical to the molecular formula of the unsymmetrical thorectidiol A diacetate (**4**). The ^{1}H and ^{13}C NMR spectra (Tables 1 and 2) recorded for the symmetrical diacetate (**5**) were similar to those obtained for thorectidiol A diacetate (**4**), except, unlike the NMR spectra of the unsymmetrical diacetate **4**, none of the resonances in the NMR spectra of the symmetrical diacetate **5** were doubled. Analysis of the 1D and 2D NMR data obtained for diacetate **5** identified the same $C_{22}H_{29}O_3$ structural fragment seen in the planar structure of the diacetate **4**, indicating that the symmetrical and unsymmetrical diacetates **4** and **5** had the same constitution **A′** but differed in configuration. As indicated above, molecular models show that the symmetrical dimer **5** must have the 9*R**,9′*R** relative configuration, which generates identical chemical environments for the C-9 and C-9′ substituents and a ^{1}H NMR spectrum with no doubling of signals.

The ^{1}H and ^{13}C NMR data acquired for thorectidol acetate (**6**) (Tables 1 and 2) were markedly similar to those obtained for the unsymmetrical and symmetrical thorectidiol diacetates **4** and **5** except for two significant differences. These differences were apparent in the resonance assigned to H-19 in the thorectidol acetate (**6**) ^{1}H NMR spectrum, which had shifted upfield to δ 6.53 compared with the corresponding H-19/H-19′ chemical shift in the symmetrical diacetate **5** at δ 6.67, and instead of being a singlet it appeared as a fine doublet in the spectrum of **6** with a *J* coupling of 2.6 Hz that showed a gCOSY

correlation to an additional aromatic doublet resonating at δ 6.46 (J = 2.6 Hz) assigned to *meta* coupling. The HRESIMS spectrum of thorectidol acetate (**6**) gave a $[M + Na]^+$ ion at *m/z* 407.2189 appropriate for a molecular formula of $C_{24}H_{32}O_4$, requiring nine sites of unsaturation, indicating that the structure of thorectidol acetate (**6**) was monomeric and the biphenyl bridge in the thorectidiol dimers had been replaced by the *meta*-coupled aromatic proton resonance at δ 6.46, assigned to H-21. gHMBC correlations between H-21 (δ 6.46) and C-11 (δ 123.0), C-17 (δ 140.7), C-19 (δ 107.1), and C-20 (δ 144.6) and tROESY correlations between H-11 (δ 6.07) and H-21 (δ 6.46) confirmed the proposed constitution of thorectidol acetate (**6**). Thorectidol (**3**) is closely related to metachromin Y recently isolated by Matsunaga's lab from the marine sponge *Spongia* (*Heterofibria*) sp. as a racemate.[10]

The unsymmetrical and symmetrical thorectidiol dimer acetates **4** and **5** and thoractidol acetate (**6**) were all isolated by normal-phase HPLC as optically inactive materials. When thorectidol acetate (**6**) was analyzed by chiral-phase HPLC, two peaks were observed in a ratio of 1:1. The ECD spectra of the two peaks were mirror images of each other, confirming that thorectidol acetate (**6**) had been isolated as a racemic mixture (Figure SI2). When the thorectidiol unsymmetrical and symmetrical dimer diacetates **4** and **5** were analyzed by chiral-phase HPLC, only two peaks were observed in a ratio of 1:1 in both cases. These peaks were collected, and the ECD spectrum for each peak was recorded (Figures SI3 and SI4). As anticipated, the ECD spectra for the dimeric biphenyl compounds show strong "split" Cotton effects centered at 231 nm, as expected for atropisomers with only weak contributions from the remote C-9/C-9′ stereogenic centers.[11,12] Upon reinjection of the material from each of the chiral-phase HPLC peaks after the samples were at room temperature for a period of several days, only single peaks were observed, ruling out the possibility of interconversion through slow rotation about the C-21/C-21′ bond of the biphenyl bridge.

Normal-phase HPLC separates the unsymmetrical thorectidiol diacetates **4** (9*R**,9′*S**) from the symmetrical thorectidiol diacetates **5** (9*R**,9*R**), and then chiral-phase HPLC separates the diacetates **4** and **5** into two peaks each that have mirror image ECD spectra (Figures SI3 and SI4). Therefore, the thoractidiol diacetates have been separated into only four distinct fractions by the sequential application of normal- and chiral-phase HPLC, which is less than the six possible stereoisomers resulting from dimers having the constitution **A′**. As described above, there are only two possible unsymmetrical thorectidiol stereoisomers with the relative configuration 9*R**,9′*S**, and these must be enantiomers that differ only in the axial configuration. Chiral-phase HPLC has separated these thorectidiol A diacetate (**4**) enantiomers to give optically pure stereoisomers. There are four possible symmetrical thorectidiol stereoisomers (Figure 2). Normal-phase HPLC only gave one peak of optically inactive material for the symmetrical dimer diacetate **5**, and chiral-phase HPLC separated this material into two peaks that gave mirror image ECD spectra (Figure SI4). There are two possible explanations for these observations. The first is that the normal-phase HPLC peak containing the symmetrical dimer contains only two stereoisomers and not the expected four and the two fractions obtained by chiral-phase HPLC purification each contain only a single stereoisomer and they are enantiomeric. However, it is more likely that the combination

of normal- and chiral-phase HPLC did not resolve the four possible symmetrical diacetate stereoisomers and that the final optically active fractions containing symmetrical thorectidiol acetates each contain two stereoisomers that have the same axial configuration but different C-9 and C-9′ configurations. Our experimental data do not distinguish between these two possibilities. However, the putative formation of the thorectidiols via phenol coupling of a racemic precursor **3** strongly supports the existence of four symmetrical stereoisomers that have not been completely resolved via the combination of normal- and chiral-phase HPLC. Despite that likelihood, given that there is no spectroscopic evidence for the isolation of more than one racemic symmetrical dimer, we have named this compound thorectidiol B (**2**), recognizing that we have not been able to assign the C-9/C-9′ and axial relative configurations.

The compounds were assessed for their ability to inhibit the RBD–ACE2 interaction using the AlphaScreen assay (Table 3). The most active compound in this assay was racemic thorectidiol A (**1**) with an IC_{50} of 1.0 ± 0.7 μM followed by racemic thorectidiol A diacetate (**4**) with an IC_{50} of 7.3 ± 2.6 μM. Both **1** and **4** also disrupted the unrelated host PD-1–PD-L1 interaction, but at much higher concentrations (respective IC_{50}'s = 6.0 ± 3.5 and 37 ± 19 μM), corresponding to selectivity indices (IC_{50} PD-1–PD-L1/IC_{50} RBD–ACE2) of 5.9 and 5.0, respectively. In contrast, minimal activity against RBD–ACE2 binding was observed for the symmetrical thorectidiol B diacetate (**5**) and thorectidol acetate (**6**), with IC_{50}'s of 65 ± 19 and 63 ± 21 μM, respectively (Table 3). (−)-Hopeaphenol, a positive control inhibitor of the RBD–ACE2 interaction, and BMS-1166, a control PD-1–PD-L1 inhibitor, blocked these respective interactions consistent with previous observations.[7] Notably, the activity of compound **1** in this assay approximated that of (−)-hopeaphenol, which in turn was demonstrated to inhibit live SARS-CoV-2 *in vitro* (e.g., half-maximal effective concentrations of 7.5–23 μM, depending on the SARS-CoV-2 variant).[7] These results suggest that the activity of compound **1** in this assay is within the range of other compounds with detectable antiviral activity, although additional amounts of this compound are needed to test this hypothesis experimentally.

In summary, the dimeric meroterpenoid thorectidiol A (**1**) isolated as a racemate from the marine sponge *D. elegans* is a selective inhibitor of the SARS-CoV-2 viral spike protein receptor binding domain interaction with the host angiotensin-converting enzyme II receptor with an IC_{50} of ≈1 μM. Thorectidiol A (**1**) is related to the dimeric monoterpene meroterpenoid scabellone A isolated from the ascidian *Aplidium scabellum*[8,13] and chromene dimers isolated from the plant *Ageratina riparia*.[14] However, we are not aware of any related dimeric meroterpenoids being reported from marine sponges or any related dimeric sesquiterpene meroterpenoids from any source. The putative formation of thorectidiol A (**1**) involves phenol coupling between two molecules of the co-occurring racemate of thorectidol (**3**), which in principle can lead to six thorectidiol stereoisomers (Figure 2). Extremely limited amounts of the crude extract that were available for study prevented the isolation of the monomer thorectidol (**3**) and the symmetrical dimer thorectidiol B (**2**) in their natural forms. Acetylation of the bulk of the crude extract facilitated the isolation of pure enantiomers of the unsymmetrical dimer thorectidiol A diacetate (**4**), a symmetrical dimer thorectidiol B diacetate (**5**), and pure enantiomers of

thorectidol acetate (**6**). The racemate of thorectidiol A diacetate (**4**) showed attenuated, but still significant, single-digit μM inhibition of the RBD/ACE2 binding interaction, while thorectidiol B diacetate (**5**) and the racemic thorectidol acetate (**6**) were only active at roughly 10-fold higher concentrations. The relative potencies of the acetylated thorectidiols demonstrate that the configuration of the dimeric stereoisomers is important for inhibition of the RBD/ACE2 binding interaction as expected.[15] Unfortunately, there were insufficient amounts of the pure thorectidiol A diacetate (**4**) enantiomers to test them for inhibition of RBD/ACE2 binding. Most often sponge meroterpenoids are isolated as single optically active stereoisomers. Interestingly, if the thorectidiol A (**1**) precursor thorectidol (**3**) had been a single enantiomer, the unsymmetrical dimer **1** (9*R**,9′*S**) could not have formed in the putative phenol coupling and the RBD/ACE2 disrupting activity of thorectidiol A (**1**) would not have been revealed.

EXPERIMENTAL SECTION

General Experimental Procedures.

Optical rotations were measured using a Jasco P-1010 polarimeter with sodium light (589 nm). UV spectra were recorded with a Waters 2998 photodiode array detector. ECD spectra were measured using a Jasco J-810 spectrophotometer with a path length of 10 mm, a bandwidth of 2 nm, a response of 4 s, a data pitch of 0.5 nm, and a scan speed of 200 nm/min. The ^{1}H and ^{13}C NMR spectra were recorded on a Bruker AV-600 spectrometer with a 5 mm CPTCI cryoprobe. ^{1}H chemical shifts are referenced to the residual C_6D_6 or DMSO-d_6 signal (δ 7.15 and 2.49, respectively), and ^{13}C chemical shifts are referenced to the C_6D_6 or DMSO-d_6 solvent peak (δ 128.0 or 39.5, respectively). Low- and high-resolution ESI-QIT-MS were recorded on a Bruker-Hewlett-Packard 1100 Esquire-LC system mass spectrometer. Merck type 5554 silica gel plates and Whatman MKC18F plates were used for analytical thin layer chromatography. Normal-phase and chiral-phase HPLC purifications were performed on a Waters 1525 binary HPLC pump attached to a Waters 2998 photodiode array detector using a flow rate of 2.0 mL/min. All solvents used for HPLC were Fisher HPLC grade and were filtered through a 0.45 μm filter (Osmonics Inc.) prior to use.

Sponge Material.

Specimens of *Dactylospongia elegans* (order Dictyoceratida, family Thorectidae) were collected by hand using scuba on September 12, 2003, near Keviang, New Ireland, Papua New Guinea (S 2°45.13′, E 150°43.09′). The sample was collected at ~30 m under an overhang. A voucher sample has been deposited at The Netherlands Centre for Biodiversity Naturalis in Leiden, The Netherlands (voucher number pending: RMNH POR. 12471).

Small-Scale Extraction of the Sponge and Isolation of Thorectidiol A (1).

Freshly collected sponge was frozen on site and transported frozen. The sponge material (10 g) was cut into small pieces and immersed in and subsequently extracted repeatedly with MeOH (3 × 25 mL) at room temperature. The combined MeOH extracts were concentrated *in vacuo*, and the resultant residue was then partitioned between EtOAc (3 × 8 mL) and H_2O (25 mL). The combined EtOAc extract was evaporated to dryness, and the resulting oil was chromatographed on Sephadex LH-20 with 4:1 MeOH/CH_2Cl_2 as eluent. Fractionation

of the resulting active material on Si gel flash chromatography (step gradient: hexanes to 1:1 hexanes/EtOAc and to MeOH, 2 g Sep Pak) resulted in a fraction eluting with 3:1 hexanes/EtOAc with activity against the spike/ACE2 interaction and a selectivity index of >10 compared with disruption of the PD-1/PD-L1 interaction. Purification of the active fraction via normal-phase HPLC, using a Alltech Apollo 5 μm, 25 × 1.0 cm column, with 1:7 acetone/hexanes as eluent gave 0.3 mg of a sample of the unsymmetrical dimer **1**.

Thorectidiol A (1):

reddish amorphous solid; UV (0.1% MeOH/CH_2Cl_2) λ_{max} 231, 273, 344 nm; ^{1}H and ^{13}C NMR, Tables 1 and 2; (−)-HRESIMS *m/z* 681.4157 $[M - H]^-$ (calcd for $C_{44}H_{57}O_6$, 681.4161).

Acetylation of Thorectidiol A (1).

To 0.2 mg of thorectidiol A (**1**) was added 0.5 mL of 1:1 Ac_2O/C_5H_5N, and the reaction stirred overnight at rt. The reaction mixture was dried and purified via normal-phase silica HPLC, using an Alltech Apollo 5 μm, 25 × 1.0 cm column, with 3:37 acetone/hexanes as eluent to yield 0.2 mg of thorectidiol A diacetate (**4**).

Thorectidiol A Diacetate (4):

pale yellow glass; UV (1.5% 2-propanol/hexanes) λ_{max} 201, 231, 269, 327 nm; ^{1}H and ^{13}C NMR, Tables 1 and 2; (+)-HRESIMS *m/z* 789.4340 $[M + Na]^+$ (calcd for $C_{48}H_{62}O_8Na$, 789.4337).

Larger Scale Extraction of the Sponge and Isolation of Thorectidiol A Diacetate (4), Thorectidiol B Diacetate (5), and Thorectidol Acetate (6).

The larger scale workup started with 40 g of sponge material and proceeded as described above, but prior to HPLC purification the active fraction was treated with 2 mL of 1:1 Ac_2O/C_5H_5N and stirred overnight at rt. The sample was then dried and fractionated via normal-phase silica HPLC, using an Alltech Apollo 5 μm, 25 × 1.0 cm column, with 3:37 acetone/hexanes as eluent to yield 1.1, 0.5, and 0.4 mg of clean samples of the thorectidiol A diacetate (**4**), thorectidiol B diacetate (**5**), and thorectidol acetate (**6**).

Thorectidiol B Diacetate (5):

clear glass; UV (1.5% 2-propanol/hexanes) λ_{max} 201, 231, 270, 327 nm; ^{1}H and ^{13}C NMR, Tables 1 and 2; (+)-HRESIMS *m/z* 789.4338 $[M + Na]^+$ (calcd for $C_{48}H_{62}O_8Na$, 789.4337).

Thorectidol Acetate (6):

pale yellow glass; UV (1.5% 2-propanol/hexanes) λ_{max} 203, 231, 268, 322 nm; ^{1}H and ^{13}C NMR, Tables 1 and 2; (+)-HRESIMS *m/z* 407.2189 $[M + Na]^+$ (calcd for $C_{24}H_{32}O_4Na$, 407.2193).

Chiral-Phase HPLC Analysis.

Using a Daicel, Chiralpak IA 5 μm, 25 × 1.0 cm column, with 1% 2-propanol/hexanes as eluent with a flow rate of 2 mL/min, the three acetates **4, 5**, and **6** were each separated into

two distinct peaks in approximately a 1:1 ratio with retentions times of 15.6/18.7, 14.7/19.2, and 17.2/18.9 min, respectively.

Calculation of the ECD Spectra of Thoretidiol A Diacetate (4).

The calculated ECD spectrum for 9*R*,9′*S*,S_a thorectidiol diacetate (**4**) (Figure SI3 panel B) is the averaged spectrum across the ECD spectra of 20 low-energy conformers of 9*R*,9′*S*,S_a thorectidiol A diacetate (**4**). The 20 low-energy conformers were selected and searched out of 1,000,000 tested conformers using Open Babel (https://open-babel.readthedocs.io/en/latest/3DStructureGen/multipleconformers.html) and Mathematica (https://reference.wolfram.com/language/guide/MolecularStructureAndComputation.html) scripts. The conformers were optimized and calculated for ECD analysis using Gaussian 16 (https://gaussian.com/td/). The ECD spectra were generated and averaged according to the Boltzmann distribution using SpecDis (https://encyclopedia.pub/entry/67).

AlphaScreen Assays.

Both RBD–ACE2 and PD-1–PD-L1 AlphaScreen assays were described previously.[7] For RBD–ACE2 interaction assays, 2 nM ACE2-Fc (Sino Biological) was incubated with 5 nM His-tagged SARS-CoV-2 spike RBD (Wuhan variant; Sino Biological) plus 5 μg/mL protein A AlphaScreen acceptor beads and 5 μg/mL nickel chelate donor beads in 20 mM Tris (pH 7.4), 150 mM KCl, and 0.05% CHAPS (3-[(3-cholamidopropyl)dimethylammonio]-1-propanesulfonate) in 10 μL reactions in 384-well format. Compounds were diluted to 100× final concentration in DMSO. A 5 μL amount of ACE2-Fc/protein A acceptor beads was added to each well, followed by 100 nL of compound dilution and 5 μL of CoV-spike-RBD-His/nickel chelate donor beads in duplicate using a Janus Nanohead tool (PerkinElmer). Reactions were incubated for 2 h at room temperature and then monitored for luminescence using a ClarioStar plate reader (BMC Labtech). Data were normalized to percent inhibition, where 100% equaled the AlphaScreen signal in the absence of SARS-CoV-2-spike-RBD-His and 0% equaled the AlphaScreen signal in the presence of both proteins and DMSO vehicle control.

For PD-1–PD-L1 interaction assays, 0.5 nM human PD-L1-Fc (Sino Biological) was incubated with 5 nM His-tagged human PD-1 (Sino Biological) in the presence of 5 μg/mL protein A AlphaScreen acceptor beads and 5 μg/mL nickel chelate donor beads in 10 μL of 20 mM HEPES (pH 7.4), 150 mM NaCl, and 0.005% Tween in 384-well format. A 5 μL sample of PD-L1-Fc/protein A acceptor beads was added to the plate first, followed by 100 nL of test compound and 5 μL of PD-1-His/nickel chelate donor beads in duplicate. Reactions were allowed to incubate for 2 h at room temperature followed by data collection as described above, where 100% equaled the AlphaScreen signal in the absence of PD-1-His and 0% equaled the AlphaScreen signal in the presence of both proteins and DMSO vehicle control alone.

For each experiment, IC_{50}'s were determined by fitting percent inhibition values to four-parameter dose–response curves using the dilution factor as the X coordinate, with the top parameter fixed to 100% and the slope constrained between 1 and 2. IC_{50} results

for compounds denote the mean ± standard deviation from at least three independent experiments, while IC_{50}'s for extracts denote the mean from a single experiment performed in duplicate.

Supplementary Material

Refer to Web version on PubMed Central for supplementary material.

ACKNOWLEDGMENTS

Financial support was supported by an NSERC Discovery grant (R.J.A., Y.A.W.), the Wistar Science Discovery Fund (L.J.M., J.S.), the Canadian Institutes for Health Research (CIHR PJT-153057) (I.T.), and a UBC Four-Year Fellowship (J.Z.). This work was also supported by the following grants to L.J.M.: Commonwealth of Pennsylvania COVID-19 funding, the Robert I. Jacobs Fund of the Philadelphia Foundation, and the Herbert Kean, M.D., Family Professorship.

REFERENCES

(1). Domingo P; Mur I; Pomar V; Corominas H; Casademont J EBiomedicine 2020, 58, 102887. [PubMed: 32736307]

(2). McKee M; Stuckler D Nat. Med 2020, 26, 640–642. [PubMed: 32273610]

(3). Meganck RM; Baric RS Nat. Med 2021, 27, 401–410. [PubMed: 33723456]

(4). Musarra-Pizzo M; Pennisi R; Ben-Amor I; Mandalari G; Sciortino MT Viruses 2021, 13, 828. [PubMed: 34064347]

(5). Hoffman M; Kleine-Weber H; Schroeder S; Kruger N; Herrier T; Erichsen S; Schiergens TS; Herrier G; Wu N-H; Nitsche A; Muller MA; Drosten C; Pohlman S Cell 2020, 181, 271–280. [PubMed: 32142651]

(6). Wrapp D; Wang N; Corbett KS; Goldsmith JA; Hsieh CJL; Abiona O; Graham BS; McLellan JS Science 2020, 367, 1260–1263. [PubMed: 32075877]

(7). Tietjen I; Cassel J; Register ET; Zhou XY; Messick T; Keeney F; Lu LD; Beattie KD; Rali T; Tebas P; Ertl HCJ; Salvino JM; David RA; Montaner LJ Antimicrob. Agents Chemother 2021, 65, No. e0077221. [PubMed: 34543092]

(8). Chan STS; Pullar MA; Khalil IM; Allouche E; Barker D; Copp BR Tetrahedron Lett. 2015, 56, 1486–1488.

(9). LaPlante SR; Fader LD; Fandrick KR; Fndrick DR; Kucke O; Kemper R; Miller PF; Edwards PJ J. Med. Chem 2011, 54, 7005–7022. [PubMed: 21848318]

(10). Hirota Y; Takada K; Ise Y; Woo SP; Inoue S; Mori N; Takikawa H; Nakamukai S; Okada S; Matsunaga S Bioorg. Med. Chem 2020, 28, 115233. [PubMed: 31848114]

(11). Person RV; Monde K; Humpf H-U; Berova N; Nakanishi K Chirality 1995, 7, 128–135. [PubMed: 7794691]

(12). Mori T; Inoue Y; Grimme S J. Phys. Chem. A 2007, 111, 4222–4234. [PubMed: 17472357]

(13). Chan STS; Pearce AN; Januario AH; Page MJ; Kaiser M; McLaughlin RJ; Harper JL; Webb VL; Barker D; Copp BR J. Org. Chem 2011, 76, 9151–9156. [PubMed: 21958335]

(14). Banerjee S; Jakupovic J; Bohlmann F; King RM; Robinson H Phytochemistry 1985, 24, 2681–2683.

(15). Zask A; Murphy J; Ellestad GA Chirality 2013, 25, 265–274. [PubMed: 23620262]

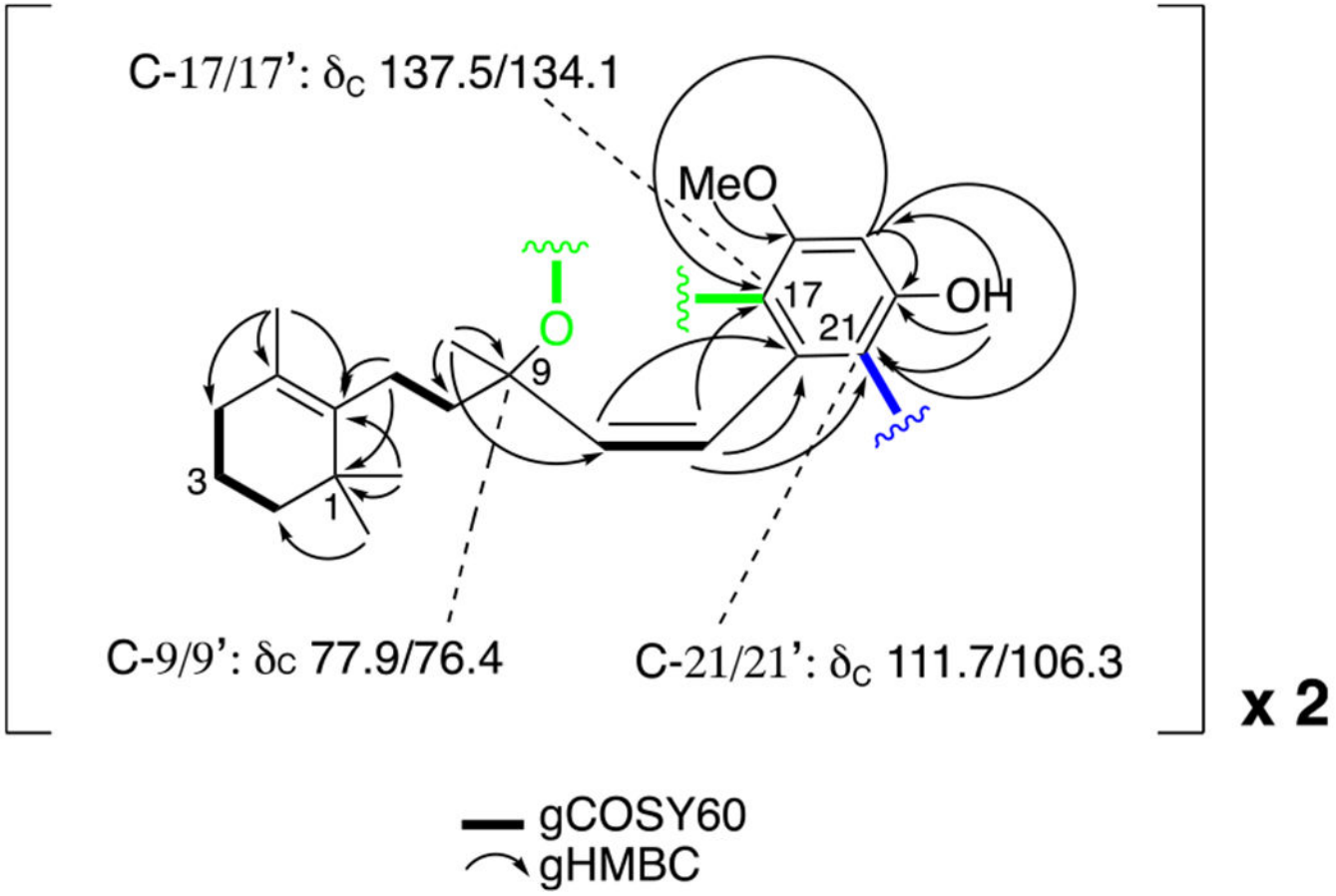

Figure 1.
Selected 2D NMR correlations observed for thorectidiol A (**1**) fragments. Biphenyl bridge in blue. Ether bridge in green.

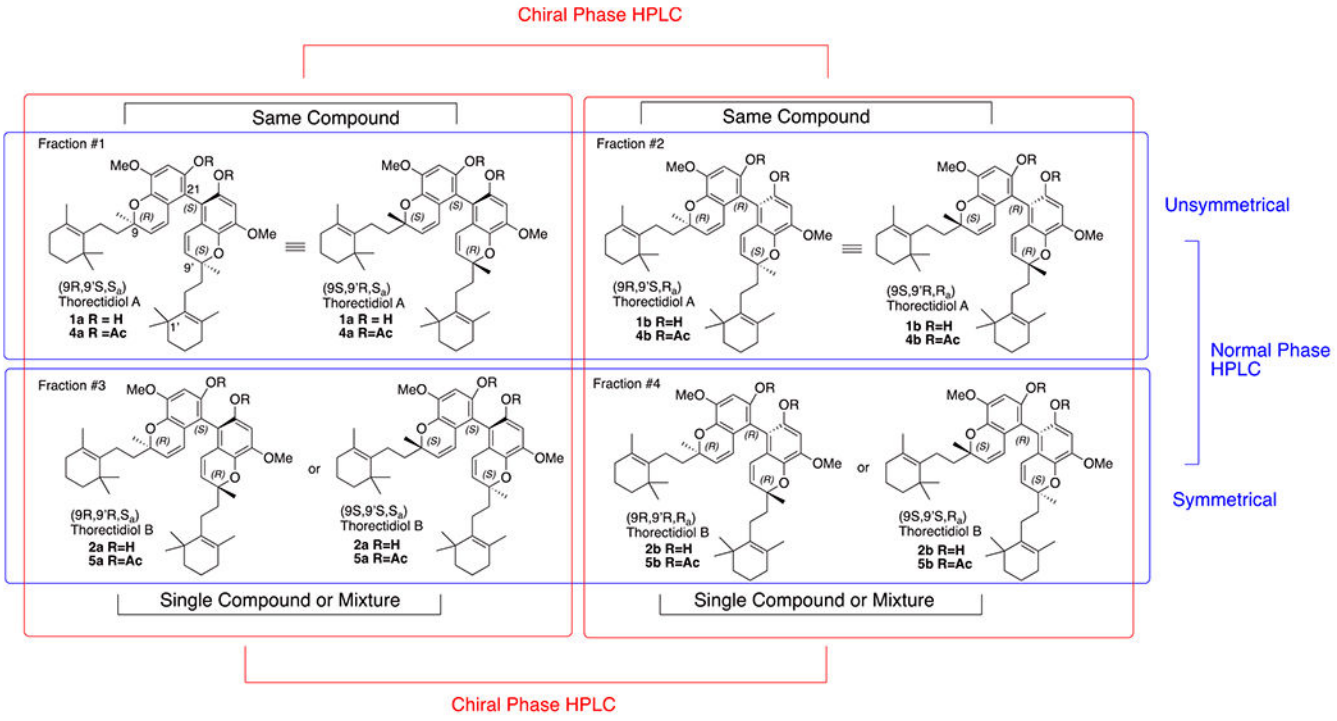

Figure 2.

Structures of the eight potential stereoisomers for the thorectidiol skeleton **A** based on the existence of atropisomerism at C-21/C-21′ and tetrahedral carbon-based stereogenic centers at C-9 and C-9′.

Table 1.

^{13}C NMR Data for Thorectidiol A (1), Thorectidiol A Diacetate (4), Thorectidiol B Diacetate (5), and Thorectidol Acetate (6) Recorded at 150 MHz

	thorectidiol A (1)		thorectidiol A diacetate (4)	thorectidiol B diacetate (5)	thorectidol acetate (6)
position	δ_C, type C_6D_6	δ_C, type DMSO-d_6	δ_C, type C_6D_6	δ_C, type C_6D_6	δ_C, type C_6D_6
1/1′	35.32/35.31, C	34.56/34.56, C	35.32/35.31, C	35.3, C	35.3, C
2/2′	40.24/40.20, CH_2	39.30/39.26, CH_2	40.29/40.23, CH_2	40.3, CH_2	40.2, CH_2
3/3′	19.96/19.94, CH_2	19.30/19.25, CH_2	19.96[a]/19.99[a], CH_2	20.0[a], CH_2	19.9[a], CH_2
4/4′	33.10/33.06, CH_2	32.19/32.16, CH_2	33.14/33.09, CH_2	33.1, CH_2	33.1, CH_2
5/5′	127.56/127.40, C	126.29/126.35, C	127.39/127.39, C	127.3, C	127.4, C
6/6′	136.95/136.87, C	136.39/136.26, C	137.89/137.10, C	137.1, C	136.9, C
7/7′	23.11/23.02, CH_2	22.09/21.96, CH_2	23.04/22.96, CH_2	23.1, CH_2	23.2, CH_2
8/8′	40.99/40.83, CH_2	39.19/39.51, CH_2	41.22/41.13, CH_2	41.4, CH_2	41.3, CH_2
9/9′	77.85/77.82, C	76.37/76.55, C	78.44/78.33, C	78.5, C	78.9, C
10/10′	131.89/131.85, CH	130.51/129.95, CH	130.84/130.83, CH	130.7, CH	130.8, CH
11/11′	121.11/121.08, CH	121.64/121.44, CH	121.65/121.54, CH	121.6, CH	123.0, CH
12/12′	28.80/28.75, CH_3	28.41/28.29, CH_3	28.88/28.81, CH_3	28.9, CH_3	28.8, CH_3
13/13′	28.73/28.67, CH_3	28.31/28.19, CH_3	28.79/28.74, CH_3	28.8, CH_3	28.7, CH_3
14/14′	19.89/19.83, CH_3	19.01/19.00, CH_3	19.93[a]/19.88[a], CH_3	19.9[a], CH_3	19.8[a], CH_3
15/15′	25.69/25.64, CH_3	25.00/24.90, CH_3	25.87/24.86, CH_3	26.0, CH_3	25.9, CH_3
16/16′	122.37/122.28, C	121.93/121.76, C	122.56/122.49, C	122.4, C	122.1, C
17/17′	137.48/137.40, C	134.09/134.23, C	140.87/140.82, C	140.9, C	140.7, C
18/18′	150.66/150.62, C	147.15/147.09, C	148.86/148.83, C	148.6, C	149.3, C
19/19′	100.92/100.83, CH	100.64/100.41, CH	107.43/107.41, CH	107.5, CH	107.1, CH
20/20′	148.97/148.88, C	148.84/148.37, C	142.99/142.95, C	143.0, C	144.6, C
21/21′	106.39/106.31, C	110.83/111.07, C	116.82/116.79, C	116.8, C	111.6, CH
18/18′-OMe	55.44/55.41, CH_3	55.50/55.40, CH_3	55.59/55.55, CH_3	55.6, CH_3	55.7, CH_3
20/20′-O(C=O)CH_3			168.75/168.88	168.8	168.6
20/20′-O(C=O)CH_3			20.43/20.46	20.6	20.6

[a]Assignments within a column are interchangeable. Chemical shifts for the thorectidiol dimers **1** and **5** are reported to two decimal places as outputted by the spectrometer to illustrate that the data for the constitutionally identical monomeric units are resolved.

Table 2.

^{1}H NMR Data for Thorectidiol A (1), Thorectidiol A Diacetate (4), Thorectidiol B Diacetate (5), and Thorectidol Acetate (6) Recorded at 600 MHz

	thorectidiol A (1)	thorectidiol A (1)	thorectidiol A diacetate (4)	thorectidiol B diacetate (5)	thorectidol acetate (6)
position	δ_H (*J* in Hz) C_6D_6	δ_H (*J* in Hz) DMSO-d_6	δ_H (*J* in Hz) C_6D_6	δ_H (*J* in Hz) C_6D_6	δ_H (*J* in Hz) C_6D_6
2/2′	1.41/1.41, m	1.33/1.33, m	1.43/1.43, m	1.44, m	1.40, m
3/3′	1.54/1.54, m	1.50–1.47	1.55/1.55, m	1.57, m	1.53, m
4/4′	1.86/1.86[a]	1.81/1.81, m	1.87/1.87[a]	1.88, t (6.3)	1.84, bt (6.2)
7/7′	2.33/2.33, bt (9.0)	2.03/2.03, m	2.44–2.31	2.40, td (13.3, 5.3)	2.34, bt (8.52)
				2.34, td (13.3, 5.1)	
8/8′	1.87/1.87[a]	1.56/1.56[a]	1.89/1.86[a]	1.90, td (13.3, 5.1)	1.86[a]
				1.84, td (13.3, 5.3)	1.79[a]
10/10′	5.39/5.38, d (10.0)	5.60/5.51, d (10.0)	5.39/5.40, d (10.0)	5.37, d (10.1)	5.35, d (9.8)
11/11′	6.13/6.12, d (10.0)	5.79/5.69, d (10.0)	6.31/6.25, d (10.0)	6.27, d (10.1)	6.07, d (9.8)
12/12′	1.06/1.06, s	0.93/0.90, s	1.09/1.06, s	1.10, s	1.06, s
13/13′	0.97/0.95, s	0.87/0.81, s	0.99/0.99, s	1.00, s	0.97, s
14/14′	1.58/1.58, s	1.47/1.44, s	1.59/1.58, s	1.61, s	1.57, s
15/15′	1.39/1.37, s	1.35/1.29, s	1.41/1.38, s	1.39, s	1.34, s
19/19′	6.53/6.51, s	6.39/6.39, s	6.68/6.66, s	6.67, s	6.53, d (2.6)
21/21′					6.46, d (2.6)
18/18′-OMe	3.37/3.37, s	3.72/3.72, s	3.39/3.38, s	3.39, s	3.30, s
20/20′-OH	4.57/4.57, bs	8.37/8.34, bs	/	/	/
20/20′-OAc			1.79/1.76, s	1.79, s	1.80, s

[a]Multiplicity not determined due to overlapping signals/chemical shifts determined from 2D data.

Table 3.

Summary Activities of Compounds on Inhibition of SARS-CoV-2 Spike RBD–Host ACE2 and Host PD-1–PD-L1 Interactions as Assessed by AlphaScreen

IC_{50} (μM)	spike RBD–ACE2 average (SD)	PD-1–PD-L1 average (SD)	selectivity index
1	1.0 (0.7)	6.0 (3.5)	5.9
4	7.3 (2.6)	37 (19)	5.0
5	65 (19)	>50	n.d.
6	63 (21)	66 (47)	1.0
(−)-hopeaphenol	0.25 (0.05)	n.d.[a]	
BMS-1166	n.d.	0.0030 (0.0023)	

[a] n.d., not determined.